BMC Medical Imaging

RESEARCH Open Access

Contrast-enhanced ultrasonography guidance avoids US-CT/MR fusion error for percutaneous radiofrequency ablation of hepatocellular carcinoma

Yang-Bor Lu[1], Yung-Ning Huang[1], Yu-Chieh Weng[1], Tung-Ying Chiang[1], Ta-Kai Fang[1], Wei-Ting Chen[1,2] and Jung-Chieh Lee[3,4*]

Abstract

Background This study evaluated the impact of contrast-enhanced ultrasonography (CEUS) combined with CT or MRI fusion imaging on percutaneous radiofrequency ablation (RFA) outcomes for hepatocellular carcinoma (HCC) inconspicuous on conventional ultrasonography (US).

Methods Patients were categorized into US-inconspicuous (USI) and US-conspicuous (USC) groups based on US imaging. The parameters of viable HCCs – including diameter, location, and RFA efficacy – were compared between USI and USC groups. Moreover, the breathing fusion imaging errors were measured. The differences in technical success, technical efficacy, local tumor progression, new tumor occurrence, and overall survival rate between USI and USC groups were analyzed.

Results Sixty-five patients with 106 lesions were included. CEUS showed high consistency with CT/MRI but revealed larger diameters ($p < 0.001$) and more feeding arteries ($p = 0.019$) than CT/MRI. Breathing fusion imaging errors averaged 17 ± 4 mm, significantly affecting lesions in segments II, III, V, and VI ($p < 0.001$). The USI group had more lesions ablated per patient in a single RFA procedure ($p = 0.001$) than the USC group. No significant differences were observed in technical success rate, technical efficacy rate, local tumor progression rate, and overall survival rate between the two groups.

Conclusions CEUS combined with fusion imaging provides detailed information on viable HCCs and their feeding arteries. CEUS-guided RFA avoids fusion imaging errors and achieves comparable efficacy in both US-conspicuous and US-inconspicuous HCCs.

Keywords Real-time fusion imaging, Contrast-enhanced ultrasonography, Hepatocellular carcinoma, Radiofrequency ablation, Inconspicuous ultrasonography

*Correspondence:
Jung-Chieh Lee
birddy@cgmh.com.cn
[1]Department of Digestive Disease, Xiamen Chang Gung Hospital Hua Qiao University, Xiamen, China
[2]Department of Gastroenterology and Hepatology, Linkou Branch, Chang Gung Memorial Hospital, Taoyuan, Taiwan
[3]Department of Ultrasound, Xiamen Chang Gung Hospital Hua Qiao University, Xiamen, China
[4]Xiamen Chang Gung Hospital, No. 123 Xiafei Road, Haicang District, Xiamen, Fujian 361028, China

Introduction

Hepatocellular carcinoma (HCC) is the fifth most prevalent malignancy and the second leading cause of cancer-related mortality worldwide [1]. Per numerous guidelines [2–4], radiofrequency ablation (RFA) has emerged as a pivotal therapeutic approach for HCC. The successful execution of RFA hinges on the accurate identification and precise targeting of viable tumors, which is challenging due to the inherent limitations of conventional ultrasonography (US). Conventional US, a common tool for HCC screening and guiding percutaneous RFA [5], has significant challenges, such as difficulties in visualizing lesions due to acoustic reflection interfaces (lung air, gastrointestinal gas, sternum, and rib), indistinct differentiation between lesions and surrounding liver parenchyma (especially concerning small HCC within the cirrhotic background), and the inability to locate residual or recurrent lesions post-treatment without contrast-enhanced ultrasonography (CEUS). Moreover, the operator's expertise plays a crucial role, demanding a comprehensive understanding of three-dimensional anatomical structures for designing an effective RFA protocol [6–8]. These constraints render conventional US inadequate for identifying HCC viable tumors and providing precise RFA guidance.

Two methods have emerged to address these challenges: Real-time Fusion imaging and CEUS [9, 10]. Fusion imaging is the process of generating new images through fusion algorithms [11, 12] and offering simultaneous visualization of US and CT/MRI images in real-time [8, 13]. Contrast-enhanced CT/MRI provides detailed information about liver lesions and their relationships with surrounding organs and extrahepatic metastatic lesions, making it the preferred imaging modality for HCC diagnosis [1]. By combining the strengths of CT/MRI and US, fusion imaging aids in localizing inconspicuous lesions on conventional US and enhances the precision of RFA guidance for HCC [14, 15]. However, our preliminary research has revealed errors in fusion imaging localization of liver lesions, exacerbated by a patient's respiratory motion and positioning changes. Hakime et al. reported a static US-CT fusion imaging error of 11.53±8.38 mm [16]. There has been no related report about fusion imaging errors caused by a patient's respiratory motions. fusion imaging errors can lead to mistarget during RFA guidance, and precise RFA guidance becomes more challenging when lesions are inconspicuous on US.

CEUS is valuable in diagnosing HCC, identifying a tumor's feeding arteries [17, 18], guiding the RFA protocol in real-time [9, 10], and following up with patients post-treatment [19]. CEUS can display viable tumors which inconspicuous on US [10]. CEUS has challenges similar to conventional US, such as acoustic reflection interface susceptibility and reliance on operator skill. Proficient sonologist can adjust patient positioning and US probe to clear display intrahepatic lesions [17].

This study aims to integrate fusion imaging with CEUS to identify US inconspicuous HCC viable tumors and monitor real-time changes in the tumor's feeding arteries. Leveraging the advantages of whole liver scanning with CT/MRI and real-time imaging with CEUS, this approach offers comprehensive visualization of viable tumors. In the context of the challenges posed by percutaneous RFA for US inconspicuous HCC, this research endeavors to employ fusion imaging combined with CEUS to provide precise RFA guidance. We hypothesize that a combination of fusion imaging with CEUS-guided RFA for US inconspicuous HCC will demonstrate a therapeutic effect comparable to that of US conspicuous HCC. Our objective is to evaluate the efficacy of a combination of fusion imaging with CEUS-guided percutaneous RFA for US inconspicuous HCC viable tumors and offer valuable clinical treatments.

Methods

Patients

This retrospective study was approved by the Xiamen Chang Gung Hospital institutional ethics review board, approval number XMCGIRB2020001. Informed consent for conducting this study was waived due to its retrospective nature. The patients diagnosed with HCC at our institution, adhering to the diagnostic criteria outlined in the Chinese [3] and AASLD [4] guidelines when viable tumor was detected during contrast-enhanced CT/MRI are enrolled. Inclusion criteria were patients (a) diagnosed with HCC scheduled for RFA; (b) with fewer than four intrahepatic HCCs; and (c) had CT/MRI performed 1–30 days before fusion imaging [16, 20]. Exclusion criteria included individuals with (a) a Child-Pugh class C; and (b) fusion imaging calibration failure due to disease progression. The patients were categorized based on a tumor that is inconspicuous on US (US inconspicuous, USI group) or conspicuous on US (US conspicuous, USC group). US inconspicuous [21] was defined as the inability of US to display and identify the viable tumor's edges, rendering it unsuitable for guiding RFA. A sonologist (J.C.L.) with over 10 years of experience performed all of the US, fusion imaging, and CEUS-guided RFA to preclude the biases. The patient's demographic data, including sex; age; hepatitis, alcoholic liver disease, and cirrhosis history; alpha-fetoprotein (AFP) levels; protein induced by vitamin K absence II (PIVKA-II); Child-Pugh class; history of previous HCC treatments; and BCLC stage [1] were documented.

Real-time fusion imaging (FI)

After reviewing the CT/MRI images (considered as reference images), the parameters of the location, maximum diameter, morphology, and high-risk characteristics of the viable tumors were documented. The viable tumor morphology was classified as circular, elliptical, or irregular. The high-risk lesions were defined as those located within 5 mm of the liver capsule, diaphragm, heart, gallbladder, digestive tract, or hepatic porta. The Digital Imaging and Communications in Medicine (DICOM) data from reference images were imported into an ultrasound machine (Logiq E9, GE Healthcare) equipped with volume navigation fusion imaging system. The optimal image sequence from the reference images (arterial or delayed phase) that provided the clearest visualization of the viable tumor was selected [20]. The GPS points at the center of the viable tumor were marked and affixed a magnetic sensor to the probe (C1-5, GE Healthcare). Then the sensor and magnetic field transmitter to the ultrasound machine's magnetic positioning device was connected. The position of the magnetic field transmitter was carefully adjusted to ensure that the US probe remained within the magnetic field space throughout the entire liver US examination.

Patients were instructed to maintain a supine position closely resembling their position during the CT/MRI examination. Fusion imaging calibration utilized a single plane and multiple-point registration. The registration plane was chosen as the transverse section of the epigastric, distinctly displaying the umbilical portion of the left portal vein. The centerline of the ultrasound beam in the ultrasound plane with the patient's midline was aligned and matched the position of the US probe to the transverse section on the reference images. For point registration, the locations as close as possible to the lesion (<30 mm), such as vascular structures or the liver surface were selected. During registration, patients were instructed to breathe slightly, and at least one full respiratory cycle was observed. The images with minimal movement (at the end of inhalation/exhalation) for point registration were selected. Two or more-point registrations were performed to complete the image registration process.

GPS point at the center of the target lesion on the reference images was precisely positioned. The fusion system recorded the magnetic field spatial position of this point and simultaneously displayed the GPS point on both the reference and real-time US images. Throughout the patient's respiratory cycle, the center of the lesion on the US image might deviate from the GPS point. The maximum distance of this deviation was defined as the breathing fusion imaging error. It was measured as follows: a GPS point at the center of the lesion on the reference images was marked and fixed the position of the US probe after displaying the GPS point in the US plane. Then the patient was asked to hold their breath. Subsequently, a point registration again to place the GPS point at the center of the lesion was performed. Once the patient resumed normal breathing, the real-time US continuously tracked the maximum deviation distance between the center of the lesion and the GPS point during the respiratory cycle. This maximum deviation distance at the end of inhalation (where the lesion moves toward the cephalic direction) and exhalation (where the lesion moves toward the caudal direction), as shown in Fig. 1, was documented as breathing fusion imaging errors. If the conventional US failed to identify the viable tumor, GPS points using the closest anatomical landmarks to the lesion (<30 mm), such as vascular structures or the liver surface was performed.

Contrast-enhanced ultrasonography (CEUS)

In this study, an ultrasound probe (C1-5, GE Healthcare) and the contrast agents SonoVue (Bracco) and Sonazoid (GE Healthcare) were employed. The US mechanical index (MI) was adjusted depending on the contrast agent used, ranging from 0.07 to 0.10 (SonoVue) and 0.2–0.3 (Sonazoid) [19, 22]. The CEUS agent was administered when both CEUS and CT/MRI images were displayed simultaneously. The CEUS images were utilized to validate the presence of viable tumors, continuously monitor tumor perfusion, and capture comprehensive images. These images were subsequently reviewed to observe and document the lesion's location, maximum diameter, morphology, high-risk characteristics, and the feeding artery. The maximum diameter during the arterial and delayed phases was recorded and compared characteristics on the CEUS with those on the reference images, encompassing factors such as location within the liver, maximum diameter, morphology, high-risk characteristics, and the presence of a feeding artery.

Percutaneous radiofrequency ablation protocol

We classified radiofrequency ablation (RFA) into two categories depending on the treatment purpose: curative intent and palliative intent, the latter involving complete ablation of the index tumor along with other known non-target tumor foci within the body [23]. The palliative RFA was employed for patients with vascular invasion, particularly portal vein tumor thrombus, who received combined hepatic arterial infusion chemotherapy (HAIC) and transarterial chemoembolization (TACE) or radiotherapy [2]; patients with multiple HCC lesions (>3 cm) who underwent TACE for larger tumors and RFA for other smaller tumors; and patients with extrahepatic metastases who underwent systemic therapy as guidelines [1, 3]. The patient positioning (left/right lateral, supine, reverse Trendelenburg position) was adjusted based

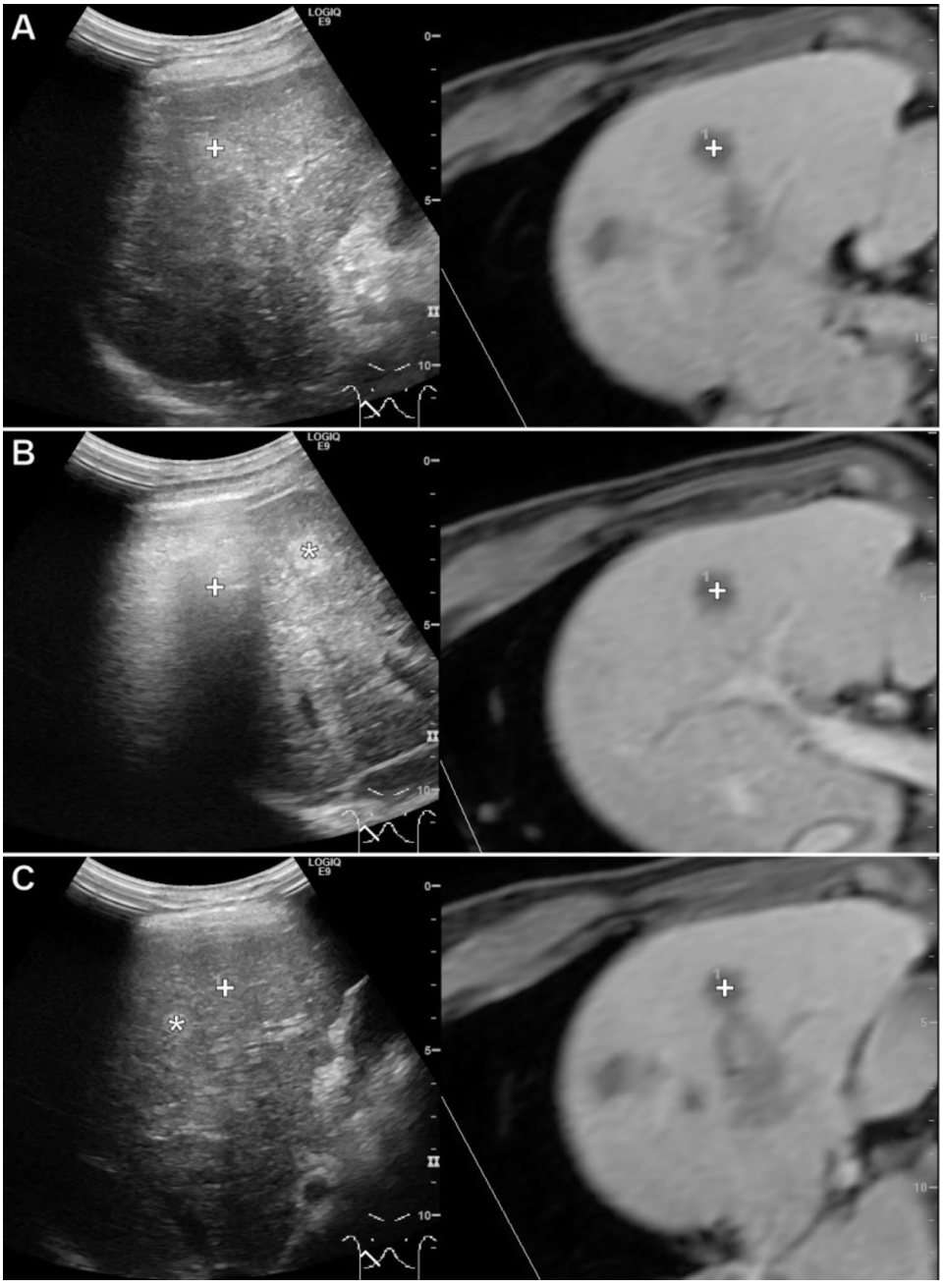

Fig. 1 Breathing fusion imaging error measurement. A patient in their 30s with a 15 mm new HCC in segment VIII after RFA. We performed real-time US-MRI fusion imaging. **(A)** Hyperechoic lesion on conventional ultrasonography (left) and low signal lesion in the delayed phase on MRI (right). The GPS point (cross mark) was set at the center of the lesion. The ultrasound probe was kept still. **(B)** When the patient inhaled deeply, real-time ultrasonography (left) showed a hyperechoic lesion (star mark) moving towards the foot side, 25 mm away from the GPS point (cross mark). **(C)** When the patient exhaled, the lesion (star mark) moved towards the cephalic side, 15 mm away from the GPS point (cross mark). The breathing fusion imaging error was 40 (25 + 15) mm. The patient was nervous with over-inhalation and exhalation, causing significant errors. After the patient engaged in several calm breathing practices, the remeasured error was reduced to 27 mm. *Abbreviations* HCC, hepatocellular carcinoma; RFA, radiofrequency ablation; US, ultrasonography; MRI, magnetic resonance imaging

on the lesion's location, ensuring optimal ultrasound access with the 3CRF probe (GE Healthcare) which is a smaller probe provides small angle access. RFA electrode insertion pathways were planned to avoid major vessels, gastrointestinal structures, and the gallbladder. The RFA electrode placement strategy was according to the intended ablation range, involving multiple overlapping ablations for larger tumors [6].

The patients were treated with a radiofrequency electrode with 20- or 30-mm active tip (ACT2020/2030,

Covidien) and an internal cooling system (Cool-tip, Covidien) attached to the radiofrequency generator. RFA was guided by CEUS. When the lesion was not clear on CEUS with the 3CRF probe, the C1-5 probe was utilized for CEUS to identify the lesion's location and peritumoral landmark [15]. The ablation procedure aimed to coagulate the tumor with an ablative margin of 5 mm for encapsulated tumors and more than 10 mm for lesions inconspicuous on US or with irregular margins. In cases of multinodular fusion type or extracapsular HCCs, the ablation zone was extended as much as possible. For hypervascular HCCs, the feeding artery was ablated before tumor ablation [18]. In cases where a high-risk lesion was located near critical organs or the hepatic dome, the techniques such as artificial ascites (5% glucose) or pleural effusion to minimize risk was employed and has the benefit to reduce acoustic interference. To ensure safety, the electrode was kept at least 5 mm distal to the gallbladder, digestive tract, and the bile duct of the portal zone. Technical success was defined as the viable tumor being covered by a hyperechoic ablation zone on US [23]. If a hyperechoic zone was not clear, the CEUS was applied.

Follow-up protocol

The technical success was evaluated by CT within 24 h after the procedure [23] and monitored patients for complications during their 48 h at the hospital. Moreover, the technical efficacy was assessed one month followed RFA with contrast-enhanced CT/MRI. Complete ablation was defined as the target tumors without enhancement and incomplete ablation was defined as the target tumors with observed enhancement. Moreover, the feasibility of repeat ablation would be evaluated. The patients were followed with repeat contrast-enhanced CT/MRI every three months during the first year and then every six months thereafter. A contrast enhancement of the tumor foci that was detected in the ablation zone (<10 mm) on follow-up CT/MRI was considerate to represent local tumor progression [23]. Patients with a new-onset tumor in other liver sites were deemed as a new tumor occurrence. Each patient's complications and overall survival has been documented.

Statistical analysis

We analyzed the data using SPSS software version 19 (SPSS, Inc., an IBM Corp., Armonk, NY, USA). The means (standard deviations) and numbers (proportions) for descriptive statistics were used to depict the distribution alternation of the outcome variables. All categorical variables were compared using Chi-square tests and continuous variables were compared using the two-sample t-test. The survival curves using a Kaplan-Meier model was generated and was compared using a log-rank test. A two-tailed P value of 0.05 was considerate to be statistically significant.

Results

Patient flow and baseline characteristics of patients

From July 2018 to June 2022, a total of 80 patients were diagnosed with viable HCC using contrast-enhanced CT/MRI (Fig. 2). Among them, nine patients were not suitable for RFA, a patient lacked DICOM data, and two had reference images taken more than 30 days prior, making them unable to obtain updated reference images. There were 68 patients who utilized real-time fusion imaging with CEUS to locate viable HCC tumors. Two of these patients did not undergo RFA; one was due to tumor progression and the other was due to lack of consent. In total, 66 patients underwent RFA. One was excluded due to loss of follow-up, leaving 65 patients with 106 viable tumors included in this study. These patients were categorized into two groups based on the conspicuity of US images: the US inconspicuous (USI) group consisted of 41 patients with 77 lesions, and the US conspicuous (USC) group consisted of 24 patients with 29 lesions. The mean interval between reference images and real-time fusion imaging was 12.0±10.1 days. Table 1 shows the detailed demographic and clinical characteristics of the patients. The median age was 56.6 years (ranges: 28–77), with 86% males. 78.5% (33 patients in USI group and 18 in USC group) had Child-Pugh class A liver function and 53.8% (23 patients in USI group and 12 in USC group) had Barcelona Clinic Liver Cancer classification (BCLC) stage B. Higher proportion of recurrent HCC in the USI group than that in the USC group ($p=0.006$). There were no significant differences between the groups in terms of sex, age, clinical data, and laboratory data.

HCC viable tumors and RFA efficacy between USI and USC groups

There were 106 viable HCC tumors included in this study, and all lesions have successfully completed fusion imaging and CEUS. There were no significant differences in lesion characteristics between the two groups (Table 2). The visual conspicuous was 27% (29/106) and inconspicuous was 73% (77/106) with US, while all lesions(100%) were identified with CEUS. The maximum diameter of the 106 lesions was 21±12 (5–64) mm with CEUS and 19±13 (5–62) mm with CT/MRI ($p<0.001$, Table S1). The discrepancy might be partly due to the CEUS being real-time rather than the reference images of CT/MRI that were performed weeks before the RFA. Despite the lesions having varying morphologies including round, oval, and irregular lesions there were highly consistent between the CEUS and reference images (kappa=0.943), the assessment of lesion locations (kappa=1), and high-risk lesions (kappa=1). The high kappa values

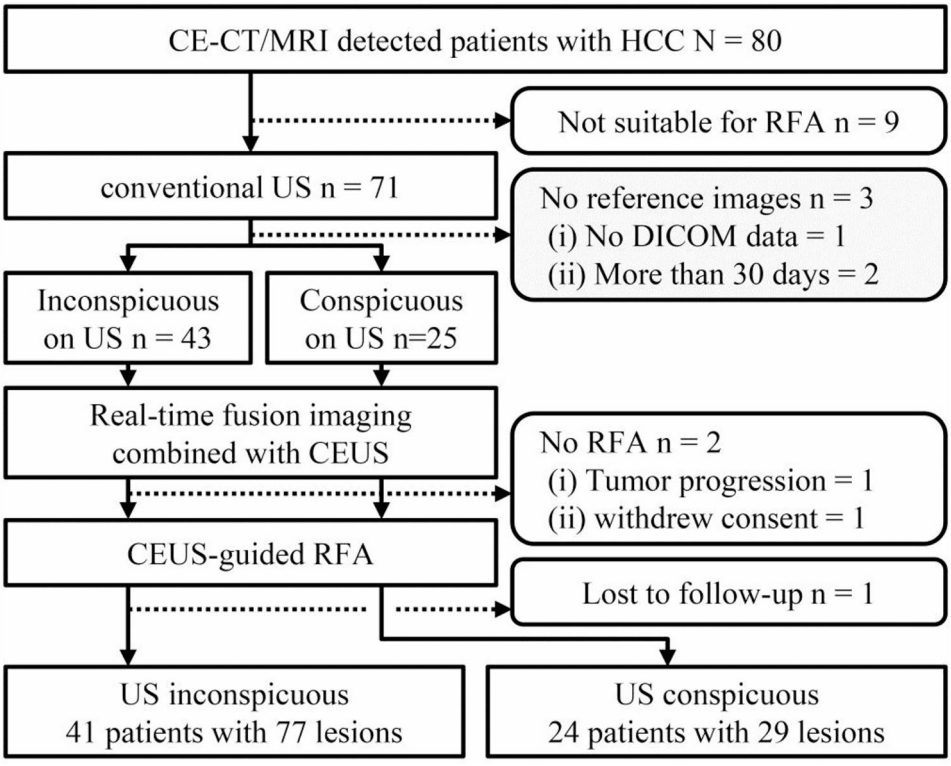

Fig. 2 Flow diagram. *Abbreviations* CE, contrast-enhanced; CT, computed tomography; MRI, magnetic resonance imaging; HCC, hepatocellular carcinoma; DICOM, digital imaging and communications in medicine; RFA, radiofrequency ablation; US, ultrasonography

(kappa=0.943-1) indicate excellent agreement between CEUS and reference images in assessing lesion morphology and location. However, CEUS detected more feeding arteries than CT/MRI (9 lesions vs. 1 lesion, respectively, $p=0.019$, Table S1), indicating a significantly higher sensitivity of CEUS in identifying vascular structures crucial for targeted RFA(shown in Fig. 3).

Table 2 illustrates the RFA parameters between the groups. A significantly greater number of lesions were ablated per patient in a single RFA procedure in the USI group compared to the USC group ($p<0.001$). There were no significant differences in the RFA electrodes, patient positioning, US probe positioning, number of electrode insertions, feeding artery ablation, and hydrodissection between the two groups. The technical success rates were both 100% in the two groups. In the USI group, one patient experienced a major post-RFA complication of a right pleural effusion and underwent drainage for palliation. In the USC group, there was one residual high-risk viable tumor identified during the one-month follow-up after the procedure. In the USI group, there were two patients with such tumors, both of whom underwent repeated RFA.

Breathing fusion imaging errors

Breathing fusion imaging errors were 17±4 (5–27) mm (Table S2). There was a significant difference in breathing fusion imaging errors between hepatic segments II, III, V, and VI and segments IV, VII, and VIII (18±4 vs. 15±4 mm, respectively, $p<0.001$, Table S2). The significant breathing fusion imaging errors observed in the liver margin, highlight the challenges in accurate lesion localization during FRA. Understanding these errors is essential for optimizing fusion imaging techniques. There was no significant breathing fusion imaging errors between the USI and USC groups (16±4 vs. 17±5 mm, respectively, $p=0.237$, Table S2, S3).

Therapqutic outcomes

Although the USI group had a higher occurrence of new tumors ($p=0.043$), there were no significant differences in technical success (both 100%), technical efficacy (97.4% vs. 96.6%, $p=0.814$), or local tumor progression (14.3% vs. 13.8%, $p=0.948$), between the USC and USI groups (Table 3). Both USI and USC groups demonstrated comparable overall survival rates ($p=0.802$, Fig. 4) and survival times of curative and palliative RFA.

Discussion

Our study was aimed to assess the efficacy of fusion imaging combined with CEUS-guided RFA for inconspicuous viable HCC and go a step further for providing valuable treatment methods and augment existing treatment modalities. Additionally, the CEUS revealed several

Table 1 Baseline patient characteristics

Characteristics	USI ($n=41$)	USC ($n=24$)	*P* value[1]
Age, y	56.4 (11.4)	56.9 (11.8)	0.864
Male	37 (90)	19 (79)	0.272
Etiology			
HBV	36 (88)	20 (79)	0.183
HCV	2 (5)	1 (4)	0.231
Alcoholic liver	4 (10)	4 (17)	0.454
Laboratory data			
Elevated AFP[2], ng/ml	17 (41)	5 (21)	0.090
Elevated PIVKA-II[3], mAU/ml	26 (63)	13 (54)	0.463
Clinical data			
Cirrhosis	41 (100)	24 (100)	1.000
Child-Pugh classification			0.270
A	33 (80)	18 (75)	
B	8 (20)	6 (25)	
BCLC stage			0.203
A	6 (15)	9 (38)	
B	23 (56)	12 (50)	
C	12 (29)	3 (13)	
Previous treatment of HCC	31 (76)	10 (42)	**0.006**
TACE	15 (37)	4 (17)	
RFA	11 (27)	3 (13)	
HAIC	4 (10)	0 (0)	
PEI	1 (2)	1 (4)	
Surgical Resection	0 (0)	2 (8)	

Continuous data are displayed as the mean (standard deviations); categorical data are expressed as the number (percentages)

Abbreviations AFP, alpha fetoprotein; BCLC, Barcelona Clinic Liver Cancer classification; HAIC, hepatic artery infusion chemotherapy; HBV, hepatitis B; HCV, hepatitis C; PEI, percutaneous ethanol injection; PIVKA-II, protein induced by vitamin K absence II; RFA, radiofrequency ablation; TACE, transcatheter arterial chemoembolization; USC, ultrasonography conspicuous; USI, ultrasonography inconspicuous

[1]To compare the groups, a two-sample *t*-test was used for the continuous variables, and chi-square tests were used for the categorical variables. Boldfaced values indicate significant differences ($P<0.05$)

[2]Defined as AFT > 20 ng/ml

[3]Defined as PIVKA-II > 40 mAU/ml

advantages, including a greater maximum diameter of viable HCC than reference images and improved visualization of the HCC arterial supply. CEUS-guided RFA could effectively avoid fusion imaging errors, particularly those associated with lesions located at the liver margin (segment II, III, V, and VI) and this method have demonstrated comparable therapeutic results between USC and USI individuals.

HCC viable tumor measurements and feeding artery observations

Our study exhibits consistency between CEUS and reference images in terms of intrahepatic locations, morphologies, and high-risk lesions of HCC viable tumors. CEUS enables real-time monitoring of viable tumor blood supply, specifically arterial phase hyperenhancement. By freely adjusting the US probe to display the maximum diameter of the viable tumor. Consequently, the maximum diameter was greater on CEUS than reference images (21 ± 12 vs. 19 ± 13 mm, respectively, $p<0.001$, Table S1); with 61% (65/106) of lesions demonstrating larger diameters with CEUS compared to the reference images. The interval between the two assessment methods was less than 30 days [16], which is feasible in clinical practice and minimizes bias in tumor growth assessment. All lesions in our study could be visualized through fusion imaging and CEUS outperformed previous research [20, 24]. Simultaneous guidance from reference images and CEUS provides enhanced visualization of the maximum viable tumor range for ablation, thereby reducing the risk of insufficient ablation and decreasing the residual cancer potential. Furthermore, real-time CEUS allows continuous and multi-dimensional observation of the morphologies and provides more detailed information about irregular viable tumors in the arterial phase as shown in Fig. 5. Upon further analysis of the differences in maximum diameter based on the location of the high-risk lesions, there were no significant differences between CEUS and reference images for lesions close to the hepatic dome ($p=0.660$). This discrepancy might be attributed to pulmonary air and rib artifacts interfering with the observation, leading to a singular dimensional

Table 2 Comparison of lesion characteristics and technical parameters between the two groups

Characteristic	USI	USC	*P* value[1]
HCC lesions, n	77	29	
CEUS diameter, mm	21(13)	22 (9)	0.603
Liver lesion location, Segment			0.538
II	7 (9)	4 (14)	
III	5 (6)	3 (10)	
IV	18 (24)	1 (3)	
V	11 (14)	5 (17)	
VI	9 (12)	4 (14)	
VII	11 (14)	4 (14)	
VIII	16 (21)	8 (28)	
High-risk lesions	51 (66)	17 (59)	0.466
RFA intent			0.088
curative	26 (63)	15 (83)	
palliative	20 (37)	3 (17)	
The number of lesions ablated per patient[2]			**0.001**
one	13 (31)	20 (83)	
two	20 (49)	4 (17)	
three	8 (20)	0 (0)	
RFA electrode			0.228
ACT 2020	31 (40)	46 (28)	
ACT 2030	8 (60)	21 (72)	
Patient positioning			0.177
Supine	19 (25)	3 (10)	
Right	45 (58)	20 (70)	
Left	9 (12)	3 (10)	
Reverse Trendelenburg's	4 (5)	3 (10)	
US probe positioning			0.625
intercostal	62 (80)	21 (73)	
epigastric	12 (16)	7 (24)	
subcostal	3 (4)	1 (3)	
Numbers of electrode insertion			0.196
one	48 (62)	15 (52)	
two	16 (21)	11 (38)	
three	11 (14)	3 (10)	
four	2 (3)	0 (0)	
Feeding artery ablation	5 (6)	4 (14)	0.253
Hydrodissection	12 (16)	8 (28)	0.159

Values are presented as the mean (standard deviations), or numbers (percentages)

Abbreviations CEUS, contrast-enhanced ultrasonography; HCC, Hepatocellular carcinoma; RFA, radiofrequency ablation; USC, ultrasonography conspicuous; USI, ultrasonography inconspicuous

[1]To compare the groups, a two-sample *t*-test was used for the continuous variables, and chi-square tests were used for the categorical variables. Boldfaced values indicate significant differences ($P<0.05$)

[2]Data are presented for the first procedure only

assessment with CEUS. Additionally, real-time CEUS enables clear and precise observation of the feeding artery in the arterial phase [17]. In our study, the feeding artery in nine lesions on CEUS was indicated, whereas only one lesion on contrast-enhanced MRI ($p=0.019$) was identified. CEUS further facilitates RFA by guiding the initial ablation for the feeding artery, thereby further improving treatment efficacy [18].

Fusion imaging errors

The accuracy of fusion imaging relies on the consistency between the reference images (CT/MRI) and the patient's anatomy. However, the patient positioning and respiratory movements during real-time fusion imaging can differ from those during reference images acquisition, leading to errors, including calibration and mistargeting errors. Some patients may have an increased risk of calibration errors. These include patients with multiple intrahepatic lesions in both the left and right lobes,

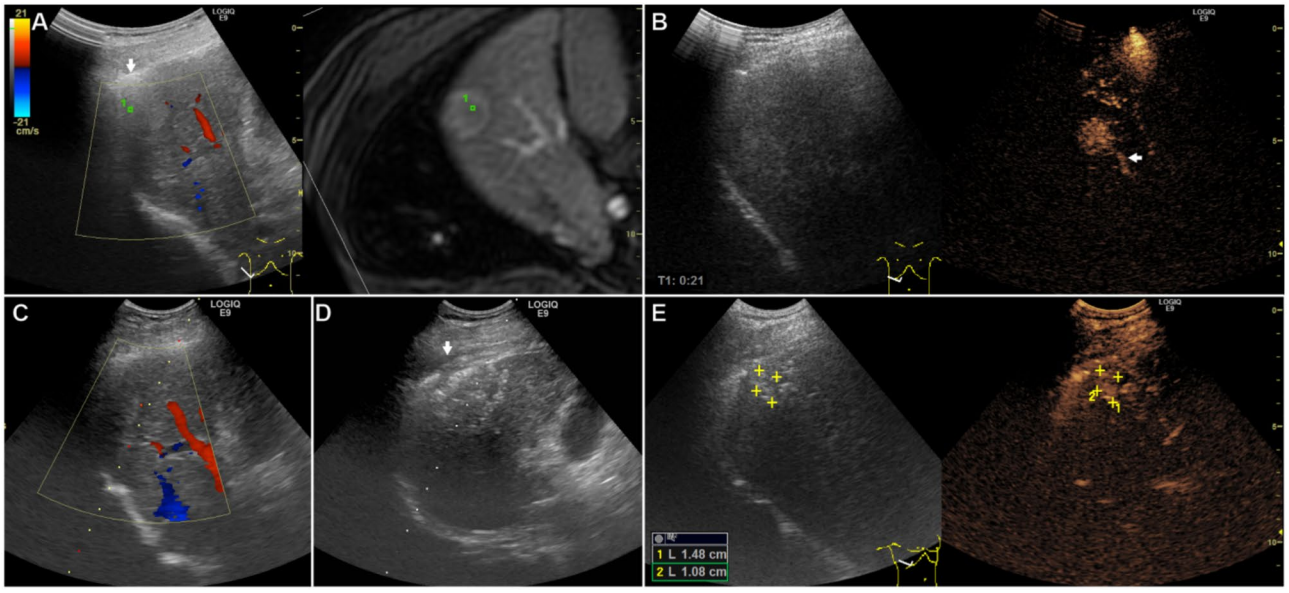

Fig. 3 A patient in their 60s with a 25 mm HCC in segment VIII near the diaphragm. **(A)** The real-time US-MRI fusion imaging showed a high-signal lesion in the arterial phase on the MRI (right) and a hyperechoic lesion on conventional US (left), which was partially occluded by pulmonary air (arrow). The GPS points (#1) of MRI and US were not fully matched due to a breathing fusion imaging error. **(B)** With the same ultrasound section as fusion imaging, the CEUS showed a feeding artery (arrow) and hyperenhancement lesion in the early arterial phase. **(C)** An RFA of the feeding artery. The patient was in the left lateral position because the electrode insertion point was too close to the bed while he was in the supine position. **(D)** Hydrodissection excluded the pulmonary air (arrow) and the patient was in the reverse Trendelenburg position. The US displayed the top of the lesion near the diaphragm. **(E)** We reinjected the contrast agent (SonoVue), and the viable tumor was hyperenhanced in the arterial phase at the top near the diaphragm. *Abbreviations* CEUS, contrast-enhanced ultrasonography; HCC, hepatocellular carcinoma; MRI, magnetic resonance imaging; RFA, radiofrequency ablation; US, ultrasonography

Table 3 Post- RFA and overall survival rates between groups

	USI group ($n=41$)	USC group ($n=24$)	*P* value[1]
Therapeutic results (%)			
Technical success rates	100.0	100.0	N.A.
Technical efficacy rates	97.4	96.6	0.814
Local tumor progression	14.3	13.8	0.948
New tumor occurrence	63.4	37.5	**0.043**
Overall survival (%)			0.802
Curative RFA			0.606
1-year	88.0	90.0	
2-year	83.8	90.0	
Palliative RFA			0.914
1-year	66.7	75.0	
2-year	33.3	25.0	
Survival times (mo)			0.802
Curative RFA	45.4 (3.9)	52.2 (4.1)	
Palliative RFA	19.0 (3.2)	18.5 (4.2)	

Values are presented as the percentages, or mean (standard deviations)

Abbreviations CEUS, contrast-enhanced ultrasonography; HCC, Hepatocellular carcinoma; mo, month; RFA, Radiofrequency ablation; N.A., not available; USC, ultrasonography conspicuous; USI, ultrasonography inconspicuous

[1]To compare between groups, chi-square tests were used for the categorical variables, and log-rank test were used for the overall survival. Boldfaced values indicate significant differences ($P<0.05$)

patients who are overweight (over 100 kg) and cause the ultrasound probe to be out of the magnetic field, and patients who have undergone a left hepatectomy and do not have the umbilical portion of the left portal vein. To address these challenges, repeated point registrations, positioned the magnetic transmitter near the probe, and alternatively utilized the splenic vein as the registration plane to reduce calibration errors. During image fusion, the position and respiratory status of a patient should be the same as possible as the reference images were acquired (as detailed in the Methods section). Previous studies have suggested performing point registrations with patients in a breath-holding state [8, 13, 16]. However, the liver displacement caused by excessive inhalation before breath-holding was observed in our study. Therefore, performing point registration when patients are in a slightly breathing status reduces calibration errors. After fusion imaging calibration, mismatches between the reference images and real-time US are mistargeting errors. These errors are primarily influenced by patients' respiratory movements, although there is no specific gauge for this measurement. In our study, breathing fusion imaging errors were 17±4 (5–27) mm. fusion imaging errors occur because the reference images are not real-time. Additionally, patients with ascites, which can increase with disease progression or decrease with

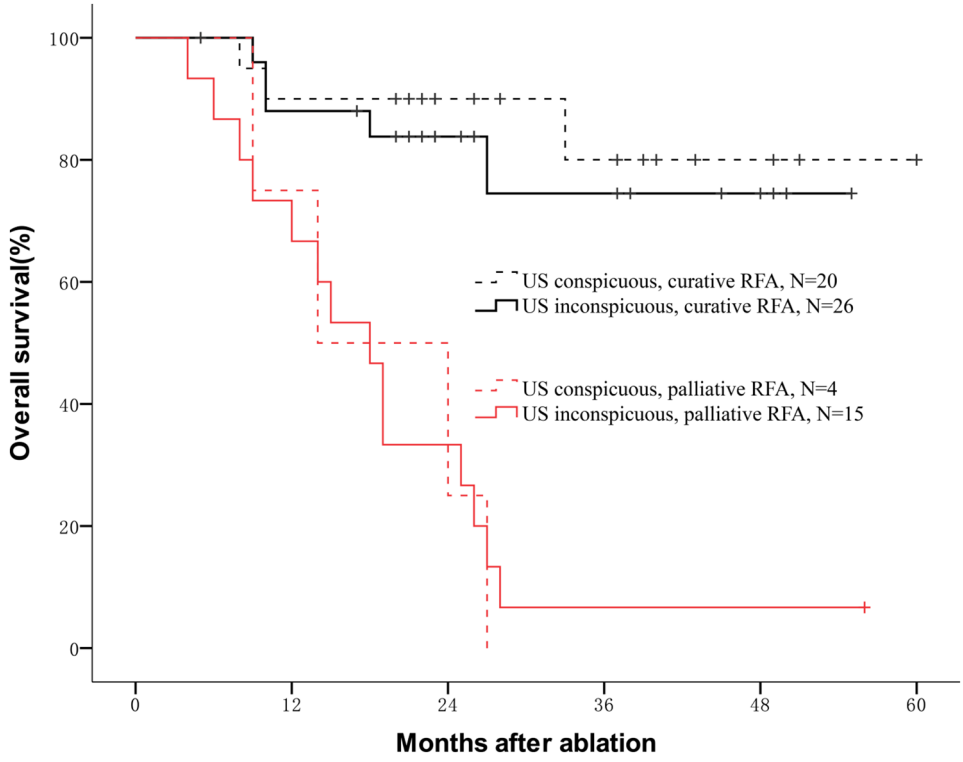

Fig. 4 A comparison of the overall survival among patients with ultrasonography inconspicuous or conspicuous hepatocellular carcinoma who underwent curative or palliative RFA. The solid and dashed lines represent the USI group and the USC group, respectively. The black and red lines represent curative and palliative RFA, respectively. *Abbreviations* RFA, radiofrequency ablation; USC, ultrasonography conspicuous; USI, ultrasonography inconspicuous

drainage, patients with increasing bowel gas, or patients with intestinal displacement may result in huge errors and failed fusion imaging calibrations [20].

CEUS-guided RFA to avoid fusion imaging errors

FI errors regarding respiratory movements are inevitable and may cause mistargeting during fusion imaging-guided RFA, especially for US inconspicuous HCCs. CEUS with simultaneous fusion imaging offers greater accuracy in lesion localization. Compared to fusion imaging-guided RFA, CEUS-guided provided real-time guidance and allowed patients positioning to be adjusted for a better RFA approach. Many circumstances benefit from CEUS-guided over fusion imaging-guided. These include patients with lesions located in liver segments II, III, V, and VI results in greater breathing fusion imaging errors ($p<0.001$) [8], patients with lesions located in the hepatic dome, the reverse Trendelenburg position could avoid pulmonary air and rib interferences for better conspicuity and RFA approach. CEUS with a smaller 3CRF probe enables the exploration of intercostal lesions from different angles, while fusion imaging with a larger C1-5 probe equipped with a magnetic sensor hinders guidance [13]. CEUS may also identify an inconspicuous lesion on the reference images (shown in Fig. 6). However, CEUS guidance could be limited by the probe. The 3CRF probe CEUS mode would make it difficult to explore the intrahepatic lesion more than 8 cm away from the probe, whereas the C1-5 probe does not have this depth limitation. Therefore, using a C1-5 probe CEUS to locate the deep lesion and then using a 3CRF to find the same US plane combined with peritumoral landmarks [15] could guide RFA for deeply inconspicuous HCC.

RFA efficacy

A higher proportion of previous recurrent HCC ($p=0.006$) were in the USI group, giving the featuring of inconspicuous and multiple lesions, which is more prone to intrahepatic metastasis with more new tumor occurrences were observed following RFA ($p=0.043$). This might explain why a greater number of lesions were ablated per patient in a single RFA procedure in the USI group ($p=0.001$). Regarding therapeutic outcomes, there were no significant differences in technical success, local tumor progression, and overall survival between the USC and USI groups. This suggests that CEUS combined with fusion imaging revealed equivalent therapeutic results among USC and USI individuals.

Suggestions to improve current US-guided RFA procedures

The current procedure has certain challenges. Conventional US without contrast-enhancement characteristics

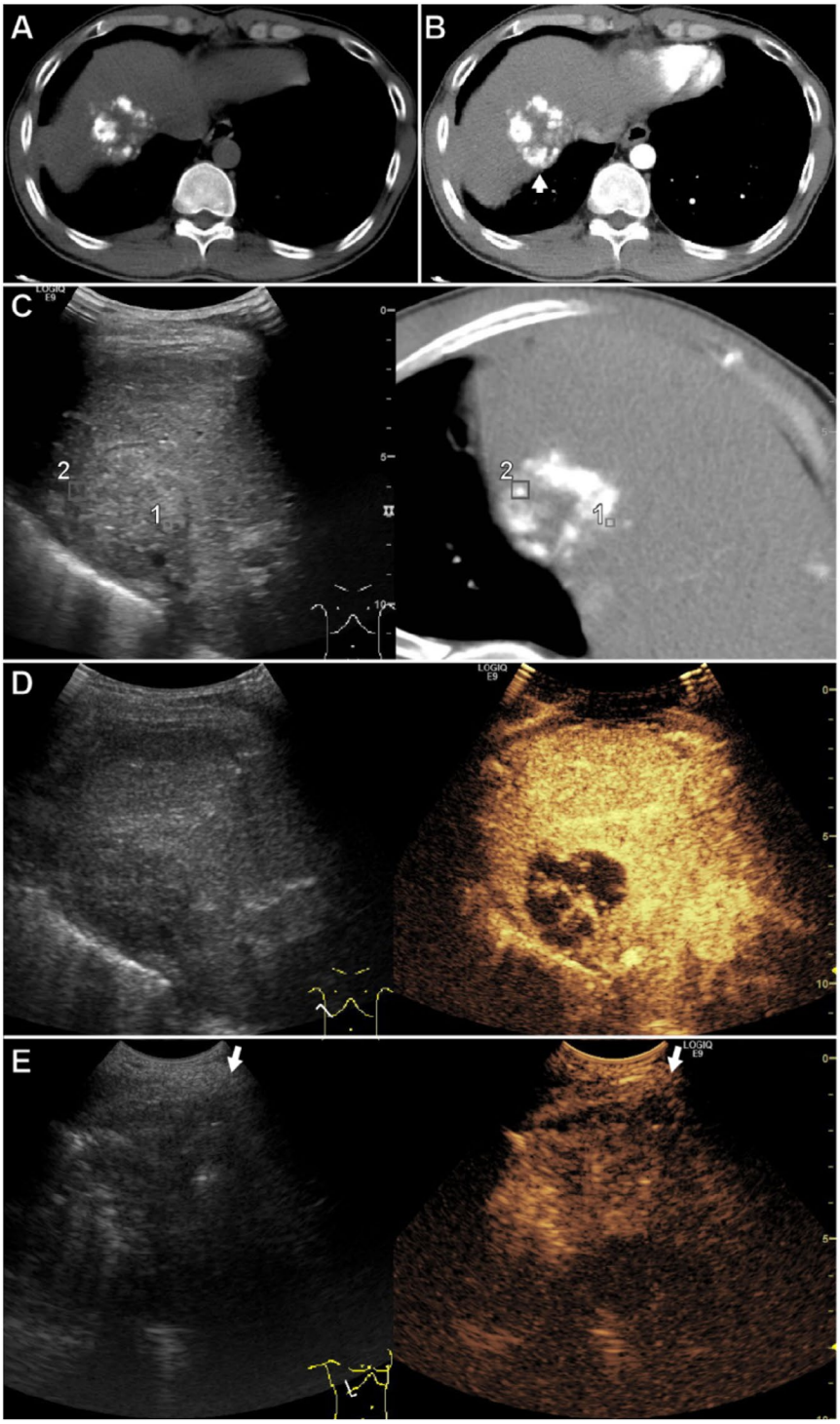

Fig. 5 A patient in their 30s with a 42 mm HCC in segment VIII after transarterial chemoembolization. **(A)** Non-enhanced CT showed high-density lipiodol partially deposited within the lesion. **(B)** Contrast-enhanced CT showed nodular enhancement (arrow) within the lesion in the arterial phase. **(C)** Real-time fusion imaging simultaneously displayed CT in the arterial phase and the US. The GPS points (#1 and #2) marked the hyper-enhanced viable tumor on CT, which is inconspicuous on US. **(D)** The CEUS showed a hyper-enhanced viable tumor in the arterial phase with the same ultrasound section as fusion imaging. The tumor was larger on CEUS than on CT. **(E)** The patient was in a left lateral position and the CEUS-guided ablated the the viable tumor. The arrow indicates the direction of the electrode insertion. Because the enhancement time is short in the arterial phase, The contrast agent (SonoVue) was reinjected to locate the viable tumor before electrode placement. *Abbreviations* HCC, hepatocellular carcinoma; CT, computer tomography; US, ultrasonography; RFA, radiofrequency ablation

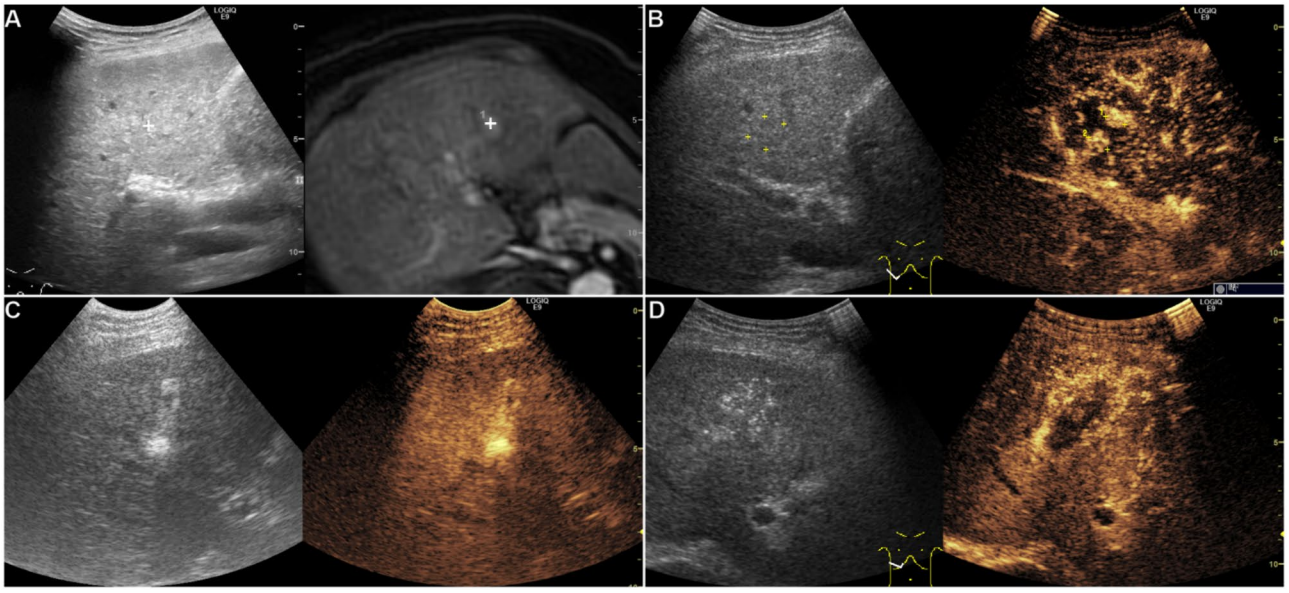

Fig. 6 A patient in their 60s with HBV cirrhosis and a new 10 mm HCC in segment IV after RFA. **(A)** Real-time fusion imaging simultaneously displayed high-signal lesions (right cross mark) in the arterial phase on MRI and inconspicuous on conventional US. **(B)** In the same US section as fusion imaging, CEUS showed two hyper-enhanced viable tumors (#1 and #2) in the arterial phase, which were inconspicuous on US and MRI (#2). **(C)** CEUS-guided RFA. **(D)** We reinjected the contrast agent (SonaZoid) after the RFA, and CEUS indicated that the tumors were covered completely by the ablation zone in the arterial phase. *Abbreviations* CEUS, contrast-enhanced ultrasonography; HBV, hepatitis B virus; HCC, Hepatocellular carcinoma; MRI, magnetic resonance imaging; RFA, Radiofrequency ablation

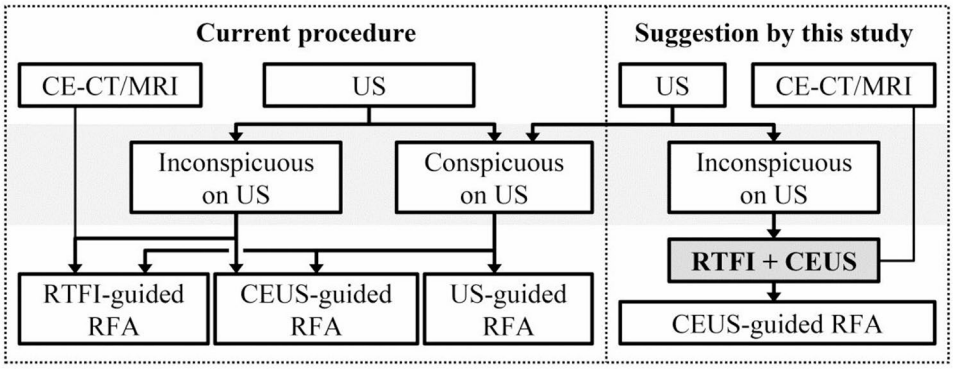

Fig. 7 Flow diagram of suggestions to improve percutaneous ultrasound-guided radiofrequency ablation. *Abbreviations* CE, contrast-enhanced; CT, computed tomography; MRI, magnetic resonance imaging; RFA, radiofrequency ablation; RTFI, real-time fusion imaging; US, ultrasonography

may fail to detect viable tumors, resulting in residual incomplete ablated tumors [9]. When lesions are inconspicuous on US, an experienced sonologist must use other reference images to determine the US probe positioning for CEUS. Fusion imaging-guided RFA restricts patients to a supine position, and there is an inevitable fusion imaging error. Mistargeting and residual tumors might occur in patients with US inconspicuous HCC guided by fusion imaging. Based on our results, fusion imaging and CEUS were suggested that the combination was able to localize inconspicuous HCCs and CEUS-guided RFA was able to avoid fusion imaging errors (Fig. 7).

This suggestion has the following benefits. Fusion imaging for inconspicuous HCC can facilitate the localization of target lesions and identify the optimal US plane [8]. The combined use of fusion imaging and CEUS enables accurate localization of the viable tumors, with CEUS providing precise information about the maximum lesion diameter and HCC feeding artery. In summary, the synergistic advantages of these two approaches enhance the accuracy of localizing recurrent HCC. For example, identifying viable tumors after TACE can be challenging due to iodized oil deposition on contrast-enhanced CT. CEUS, unaffected by iodized oil, can accurately localize viable tumors and feeding arteries, thereby increasing the technical success of RFA. Besides, CEUS offers real-time

imaging to avoid fusion imaging errors and allows patient positioning change.

Sterntghs of our study

Our study presents several novel contributions to the field of HCC percutaneous RFA. First quantification of breathing fusion imaging errors. To the best of our knowledge, this is the first study to report and detailed measure breathing-induced fusion imaging errors that can lead to mistargeting during RFA guidance. Previous studies [20, 24, 25] have not addressed this challenge. By quantifying these errors (mean error of 17±4 mm), particularly significant in lesions located in segments II, III, V, and VI, were able to minimize mistargeting and enhance the accuracy of RFA procedures. Second, improved tumor conspicuity with CEUS following fusion imaging. We demonstrated that implementing CEUS following fusion imaging significantly improved tumor conspicuousness, especially for inconspicuous tumors on US without contrast. This enhancement is critical for accurate localization and effective treatment of HCC lesions that are difficult to identify with conventional imaging techniques. Third, the role of real-time CEUS in avoiding fusion imaging errors. Real-time CEUS plays a significant role in avoiding fusion imaging errors during RFA guidance. Tumors could change over time or with the patient's position, and the delay between preoperative reference imaging and the actual RFA procedure may lead to inaccuracies in targeting. By providing immediate visualization of the tumor at the time of treatment, real-time CEUS addresses the risks associated with tumor growth or displacement between reference images and RFA, ensuring precision localization and enhancing the ablation effectiveness. Building upon the existing literature, our research fills a gap in current practices, where conventional US (without contrast) and fusion imaging alone may be insufficient for patients with poorly identifiable lesions. This combined approach has demonstrated its efficacy and feasibility. Specifically, it overcomes the challenges posed by inconspicuous tumors on US, allowing these patients to become elgible for RFA and achieve comparable therapeutic outcomes.

Potential limitations

We acknowledge that selection bias is inherent in this study, as only lesions visible on contrast-enhanced CT/MRI could be included. For example, patients diagnosed with HCC who underwent TACE might have viable tumors detected by CEUS that were not demonstrated on contrast-enhanced CT due to iodized oil. This limitation reflects the constraints of current imaging technologies and underscores the need for further advancement in imaging methods to reduce such biases. Furthermore, Integrating multiple imaging layers introduces computational complexity that may affect procedural efficiency. Parallel computation methods, such as those described in recent studies [26–29], could potentially mitigate these challenges by enhancing processing speed and efficiency. In addition, variability in liver shape, size, and texture presents challenges in medical imaging. Preprocessing steps and regularization techniques could improve imaging robustness and segmentation accuracy [30–33]. Thus, while our current focus is on the clinical application of CEUS-guided RFA, further research should explore these computational strategies to address the limitations identified. This could lead to improved imaging techniques that enhance the accuracy and efficiency of HCC treatment.

Conclusions

CEUS combined with fusion imaging provides detailed information on viable tumors and their feeding arteries, particularly for inconspicuous HCC on conventional US. CEUS plays a crucial role in RFA guidance, avoids fusion imaging errors, and showed similar therapeutic outcomes for both USI and USC individuals.

The distinguishing aspects of our study not only improve efficacy and safety [25] but also expand the application for treatment. By addressing breathing-induced errors and enhancing tumor visualization, our approach facilitates more accurate and effective treatments for patients who were previously considered unsuitable candidates for percutaneous RFA due to inconspicuous lesions. Future research should focus on combining multiple imaging techniques other than CT/MRI, which could expand the indications for percutaneous RFA, offering more patients access to minimally invasive treatments with improved precision and outcomes.

Abbreviations

AFP	alpha fetoprotein
BCLC	Barcelona Clinic Liver Cancer classification
CEUS	contrast-enhanced ultrasonography
CT	computed tomography
DICOM	digital imaging and communications in medicine
HAIC	hepatic artery infusion chemotherapy
HBV	hepatitis B virus
HCC	Hepatocellular carcinoma
HCV	hepatitis C virus
MRI	magnetic resonance imaging
PEI	percutaneous ethanol injection
PIVKA-II	protein induced by vitamin K absence II
RFA	radiofrequency ablation
TACE	transcatheter arterial chemoembolization
US	ultrasonography
USC	ultrasonography conspicuous
USI	ultrasonography inconspicuous

Supplementary Information

The online version contains supplementary material available at https://doi.org/10.1186/s12880-024-01508-w.

Supplementary Material 1

Acknowledgements
We sincerely thank Professor Sheng-Nan Lu from the Department of Internal Medicine and the deputy-superintendent of the Kaohsiung Chang Gung Memorial Hospital (CGMH), for his support in establishing our research in the field of hepatitis and hepatocellular carcinoma studies and for his guidance in mastering RFA techniques. Additionally, we would like to express our special gratitude to Dr. Sandy Hui-Shan Hsieh for her invaluable assistance in editing this paper.

Author contributions
Yang-Bor Lu: Conceptualization, Investigation, Methodology, Writing – review & editing, Supervision. Yung-Ning Huang: Conception and Design, Writing-original draft preparation. Yu-Chieh Weng: Conception and Design, Methodology, Writing-original draft preparation. Tung-Ying Chiang: Conception and Design, Writing-original draft preparation. Ta-Kai Fang: Conception and Design, Writing-original draft preparation. Wei-Ting Chen: Investigation, Methodology, Writing – review & editing. Jung-Chieh Lee: Conceptualization, Data curation, Formal analysis, Investigation, Methodology, Funding acquisition, Writing – original draft, Writing – review & editing.

Funding
This research was supported by Fujian provincial health technology project (Grant No. 3502Z20194094) and Xiamen Chang Gung hospital Fund (Grant No. CMRPG1G0151) for the conduct of the study. They had no role in the study design, data collection and analysis, decision to publish, or preparation of the manuscript.

Data availability
The data that support the findings of this study are available from the corresponding author upon reasonable request.

Declarations

Ethics approval and consent to participate
The current study was approved by the institutional ethics review board of Xiamen Chang Gung Hospital. Informed consent for conducting this study was waived due to its retrospective nature. The authors declare that this report does not contain any personal information that could lead to identification.

Consent for publication
Not applicable.

Competing interests
The authors declare no competing interests.

Clinical trial number
Not applicable.

Received: 21 July 2024 / Accepted: 20 November 2024
Published online: 28 November 2024

References

1. Wen N, Cai Y, Li F, Ye H, Tang W, Song P, Cheng N. The clinical management of hepatocellular carcinoma worldwide: a concise review and comparison of current guidelines: 2022 update. Biosci Trends. 2022;16(1):20–30.
2. Shao YY, Wang SY, Lin SM, Diagnosis G, Systemic Therapy G. Management consensus guideline for hepatocellular carcinoma: 2020 update on surveillance, diagnosis, and systemic treatment by the Taiwan Liver Cancer Association and the Gastroenterological Society of Taiwan. J Formos Med Assoc. 2021;120(4):1051–60.
3. Xie DY, Ren ZG, Zhou J, Fan J, Gao Q. 2019 Chinese clinical guidelines for the management of hepatocellular carcinoma: updates and insights. Hepatobiliary Surg Nutr. 2020;9(4):452–63.
4. Heimbach JK, Kulik LM, Finn RS, Sirlin CB, Abecassis MM, Roberts LR, Zhu AX, Murad MH, Marrero JA. AASLD guidelines for the treatment of hepatocellular carcinoma. Hepatology. 2018;67(1):358–80.
5. Yang W, Yan K, Goldberg SN, Ahmed M, Lee JC, Wu W, Zhang ZY, Wang S, Chen MH. Ten-year survival of hepatocellular carcinoma patients undergoing radiofrequency ablation as a first-line treatment. World J Gastroenterology: WJG. 2016;22(10):2993–3005.
6. Chen MH, Yang W, Yan K, Zou MW, Solbiati L, Liu JB, Dai Y. Large liver tumors: protocol for radiofrequency ablation and its clinical application in 110 patients–mathematic model, overlapping mode, and electrode placement process. Radiology. 2004;232(1):260–71.
7. Yang W, Yan K, Wu GX, Wu W, Fu Y, Lee JC, Zhang ZY, Wang S, Chen MH. Radiofrequency ablation of hepatocellular carcinoma in difficult locations: strategies and long-term outcomes. World J Gastroenterology: WJG. 2015;21(5):1554–66.
8. Lee MW. Fusion imaging of real-time ultrasonography with CT or MRI for hepatic intervention. Ultrasonography. 2014;33(4):227–39.
9. Chen MH, Yang W, Yan K, Dai Y, Wu W, Fan ZH, Callstrom MR, Charboneau JW. The role of contrast-enhanced ultrasound in planning treatment protocols for hepatocellular carcinoma before radiofrequency ablation. Clin Radiol. 2007;62(8):752–60.
10. Kim AY, Lee MW, Rhim H, Cha DI, Choi D, Kim YS, Lim HK, Cho SW. Pretreatment evaluation with contrast-enhanced ultrasonography for percutaneous radiofrequency ablation of hepatocellular carcinomas with poor conspicuity on conventional ultrasonography. Korean J Radiol. 2013;14(5):754–63.
11. Peng G, Wang Z, Zhang Z, Xiao Z. Image fusion by pulse couple neural network with shearlet. Opt Eng. 2012;51:7005.
12. Geng P, Sun X, Liu J. Adopting Quaternion Wavelet transform to fuse Multimodal Medical images. J Med Biol Eng. 2017;37(2):230–9.
13. Toshikuni N, Tsutsumi M, Takuma Y, Arisawa T. Real-time image fusion for successful percutaneous radiofrequency ablation of hepatocellular carcinoma. J Ultrasound Medicine: Official J Am Inst Ultrasound Med. 2014;33(11):2005–10.
14. Lee CH, Chen WT, Lin CC, Teng W, Lin SM, Chiu CT. Radiofrequency ablation assisted by real-time virtual sonography for hepatocellular carcinoma inconspicuous under sonography and high-risk locations. Kaohsiung J Med Sci. 2015;31(8):413–9.
15. Huang HC, Gatchalian LB, Hsieh YC, Chen WT, Lin CC, Lin SM. Real-time virtual sonography-assisted radiofrequency ablation in liver tumors with conspicuous or inconspicuous images or peritumoral landmarks under ultrasonography. Abdom Radiol (NY). 2021;46(6):2814–22.
16. Hakime A, Deschamps F, De Carvalho EG, Teriitehau C, Auperin A, De Baere T. Clinical evaluation of spatial accuracy of a fusion imaging technique combining previously acquired computed tomography and real-time ultrasound for imaging of liver metastases. Cardiovasc Intervent Radiol. 2011;34(2):338–44.
17. Lee JC, Yan K, Lee SK, Yang W, Chen MH. Focal liver lesions: real-time 3-Dimensional contrast-enhanced Ultrasonography compared with 2-Dimensional contrast-enhanced Ultrasonography and magnetic resonance imaging. J Ultrasound Medicine: Official J Am Inst Ultrasound Med. 2017;36(10):2015–26.
18. Zhang ZY, Lee JC, Yang W, Yan K, Wu W, Wang YJ, Chen MH. Percutaneous ablation of the tumor feeding artery for hypervascular hepatocellular carcinoma before tumor ablation. Int J Hyperth. 2018;35(1):133–9.
19. Dietrich CF, Nolsoe CP, Barr RG, Berzigotti A, Burns PN, Cantisani V, Chammas MC, Chaubal N, Choi BI, Clevert DA, et al. Guidelines and good clinical practice recommendations for contrast enhanced Ultrasound (CEUS) in the liver - update 2020 - WFUMB in Cooperation with EFSUMB, AFSUMB, AIUM, and FLAUS. Ultraschall Med. 2020;41(5):562–85.
20. Lee MW, Rhim H, Cha DI, Kim YJ, Choi D, Kim YS, Lim HK. Percutaneous radiofrequency ablation of hepatocellular carcinoma: fusion imaging guidance for management of lesions with poor conspicuity at conventional sonography. AJR Am J Roentgenol. 2012;198(6):1438–44.
21. Lee MW, Lim HK, Rhim H, Cha DI, Kang TW, Song KD, Min JH, Gwak GY, Kim S, Lu DSK. Percutaneous Radiofrequency Ablation of Small (1–2 cm) Hepatocellular Carcinomas Inconspicuous on B-Mode Ultrasonographic Imaging: Usefulness of Combined Fusion Imaging with MRI and Contrast-Enhanced Ultrasonography. *Can J Gastroenterol Hepatol* 2018, 2018:7926923.
22. Lee JY, Minami Y, Choi BI, Lee WJ, Chou YH, Jeong WK, Park MS, Kudo N, Lee MW, Kamata K, et al. The AFSUMB Consensus statements and recommendations for the clinical practice of contrast-enhanced ultrasound using Sonazoid. Ultrasonography. 2020;39(3):191–220.

23. Ahmed M, Solbiati L, Brace CL, Breen DJ, Callstrom MR, Charboneau JW, Chen MH, Choi BI, de Baere T, Dodd GD. Image-guided tumor ablation: standardization of terminology and reporting criteria–a 10-year update. Radiology. 2014;273(1):241–60. 3rd et al.
24. Ahn SJ, Lee JM, Lee DH, Lee SM, Yoon JH, Kim YJ, Lee JH, Yu SJ, Han JK. Real-time US-CT/MR fusion imaging for percutaneous radiofrequency ablation of hepatocellular carcinoma. J Hepatol. 2017;66(2):347–54.
25. Jie T, Guoying F, Gang T, Zhengrong S, Maoping L. Efficacy and Safety of Fusion Imaging in Radiofrequency Ablation of Hepatocellular Carcinoma Compared to Ultrasound: a Meta-analysis. Front Surg. 2021;8:728098.
26. Zhai X, Chen M, Esfahani SS, Amira A, Bensaali F, Abinahed J, Dakua S, Richardson RA, Coveney PV. Heterogeneous system-on-chip-based lattice-boltzmann visual Simulation System. IEEE Syst J. 2020;14(2):1592–601.
27. Esfahani SS, Zhai X, Chen M, Amira A, Bensaali F, AbiNahed J, Dakua S, Younes G, Baobeid A, Richardson RA, et al. Lattice-boltzmann interactive blood flow simulation pipeline. Int J Comput Assist Radiol Surg. 2020;15(4):629–39.
28. Zhai X, Amira A, Bensaali F, Al-Shibani A, Al-Nassr A, El-Sayed A, Eslami M, Dakua SP, Abinahed J. Zynq SoC based acceleration of the lattice boltzmann method. Concurrency Computation: Pract Experience. 2019;31(17):e5184.
29. Zhai X, Eslami M, Hussein ES, Filali MS, Shalaby ST, Amira A, Bensaali F, Dakua S, Abinahed J, Al-Ansari A, et al. Real-time automated image segmentation technique for cerebral aneurysm on reconfigurable system-on-chip. J Comput Sci. 2018;27:35–45.
30. Ansari MY, Yang Y, Meher PK, Dakua SP. Dense-PSP-UNet: a neural network for fast inference liver ultrasound segmentation. Comput Biol Med. 2023;153:106478.
31. Ansari MY, Chandrasekar V, Singh AV, Dakua SP. Re-routing drugs to blood brain barrier: a Comprehensive Analysis of Machine Learning approaches with fingerprint amalgamation and data balancing. IEEE Access. 2023;11:9890–906.
32. Mohanty S, Dakua SP. Toward Computing Cross-modality symmetric Non-rigid Medical Image Registration. IEEE Access. 2022;10:24528–39.
33. Ansari MY, Yang Y, Balakrishnan S, Abinahed J, Al-Ansari A, Warfa M, Almokdad O, Barah A, Omer A, Singh AV, et al. A lightweight neural network with multiscale feature enhancement for liver CT segmentation. Sci Rep. 2022;12(1):14153.

Publisher's note